GEOMETRIC MODELING AND AERODYNAMIC ANALYSIS OF THE RR LENTUS MOTOR GLIDER

Liviu BUCUR, Cristina LUPULEASA

"Henri Coandă" Air Force Academy, Braşov, Romania (bucurliviu3@gmail.com, cristinalupuleasa13@gmail.com)

DOI: 10.19062/1842-9238.2026.24.1.4

Abstract: *This research presents a systematic aerodynamic evaluation of the RR Lentus motor glider through a digital reverse engineering workflow. Due to the absence of proprietary manufacturer data, the study focuses on reconstructing a high-fidelity digital twin to predict flight behavior and stability characteristics. The methodology integrates geometric acquisition via photogrammetry with specialized design tools, utilizing winghelper for structural visualization and xflr5 for computational fluid dynamics (CFD) analysis based on the vortex lattice method (VLM). The analysis follows a dual-stage approach: a 2D analysis of the NACA 4407 and NACA 0009 airfoils to determine section polars, followed by a comprehensive 3D simulation of the full aircraft assembly. Key performance metrics, including the total lift-to-drag ratio (C_l/C_d) and longitudinal stability derivatives, were quantified under international standard atmosphere (ISA) conditions. Furthermore, a detailed mass-moment analysis was conducted to localize the center of gravity (CG) at 33% of the mean aerodynamic chord (MAC), ensuring a balanced flight envelope. The findings provide a technical baseline for the aerodynamic validation of high-performance RC gliders, demonstrating the efficacy of open-source simulation tools in academic UAV research.*

Keywords: *analysis, reverse engineering, WingHelper, XFLR5, Vortex Lattice Method.*

Symbols and acronyms:

C_l	Lift coefficient	VLM	Vortex Lattice Method
C_d	Drag coefficient	Re	Reynolds number
C_l/C_d	Lift-to-drag ratio	UAV	Unmanned Aerial Vehicle
C_L	Total lift coefficient	MAC	Mean aerodynamic chord
C_D	Total drag coefficient	AoA (α)	Angle of Attack
C_L/C_D	Total lift-to-drag ratio	MTOW	Maximum Take-Off Weight
CG	Center of gravity	ESC	Electronic Speed Controller
RC	Radio Control	CAD	Computer-Aided Design
CFD	Computational Fluid Dynamics	OEM	Original Equipment Manufacturer
NACA	National Advisory Committee for Aeronautics	ISA	International Standard Atmosphere

1. INTRODUCTION

The study of contemporary radio-controlled (RC) aircraft necessitates a shift from observational testing toward theoretical validation. This research focuses on the RR Lentus, a high-performance motor glider developed by Multiplex specifically for thermal soaring and slope soaring applications. According to manufacturer specifications, the aircraft incorporates an advanced airfoil design that facilitates a broad dynamic flight envelope and controlled landings through a four-flap "butterfly" (crow) configuration [1].

In its standard Ready-for-Radio (RR) iteration, the model is equipped with a ROXXY brushless power system optimized for 3S LiPo configurations, utilizing six Hitec HS-65HB servos to actuate the primary control surfaces: elevator, rudder, ailerons and flaps. While Multiplex provides this baseline operational parameters-along with options for aerotow releases or retractable landing gear, the full suite of aerodynamic coefficients remains proprietary and is not publicly documented.

The primary objective of this study is to address this informational deficit by synthesizing the missing technical parameters through high-fidelity simulation. Moving beyond the general descriptions provided by the manufacturer, this paper adopts a reverse engineering methodology. By digitizing the physical geometry of the airframe and performing a computational analysis within the XFLR5 environment, we aim to establish a quantitative baseline for the aircraft's longitudinal stability and aerodynamic efficiency.

2. METHODOLOGY AND GEOMETRIC RECONSTRUCTION

A precise digital replica of the RR Lentus was engineered to ensure the accuracy of the subsequent aerodynamic evaluations. Given that proprietary CAD data is unavailable, the model was reconstructed using an integrated three-phase workflow: photogrammetry for geometric capture, structural definition and the final aerodynamic modeling.

2.1 Geometric acquisition. To facilitate the 3D reconstruction, the model's geometry was first mapped using ImageOnline (Fig. 1) [2]. A top-down photographic analysis, calibrated against the 3000 mm wingspan, allowed for the precise identification of chord lengths and sweep angles at multiple stations, forming the structural basis of the simulation model.

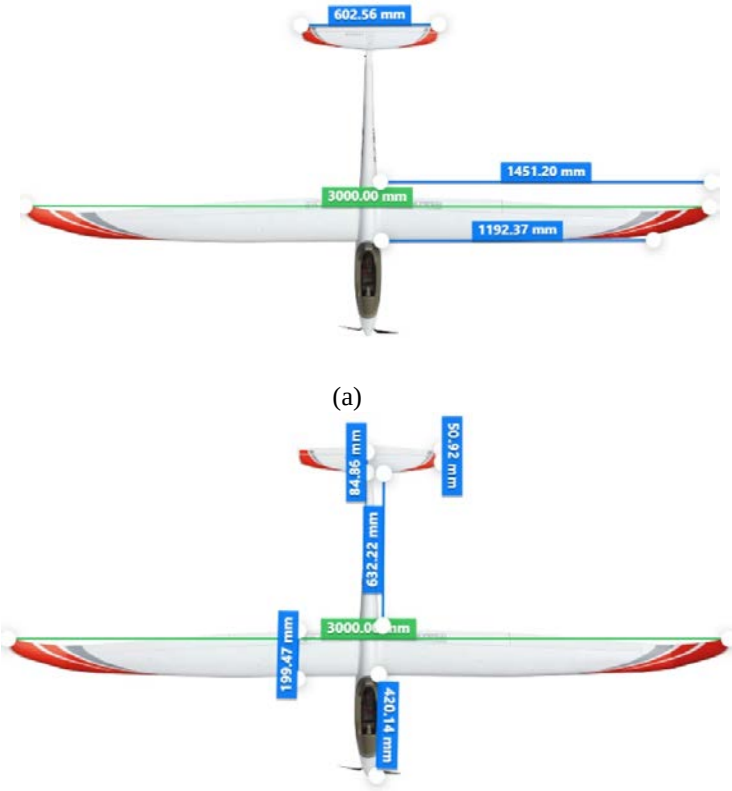

(a)

(b)

FIG. 1 Geometric acquisition and dimensioning using ImageOnline

2.2 Structural and propeller modeling. Based on the extracted measurements, the wing geometry was visualized using WingHelper [3]. This software allowed for the definition of the aerodynamic surfaces, including the dihedral angles and the placement of control surfaces (Fig. 2). The wing employs a classic rib-and-spar construction. The aerodynamic profile is defined by a series of ribs, generated according to the NACA 4407 coordinates [4], featuring lightening holes to optimize the strength-to-weight ratio. The primary aerodynamic loads are carried by a dual-spar system (upper and lower caps connected by shear webbing) running spanwise, designed to resist bending moments during flight.

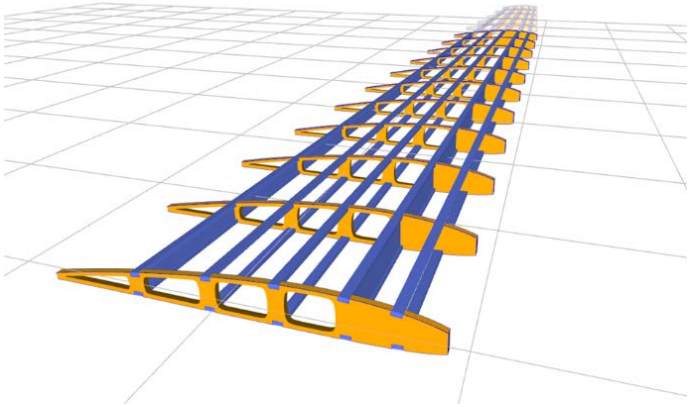

(a)

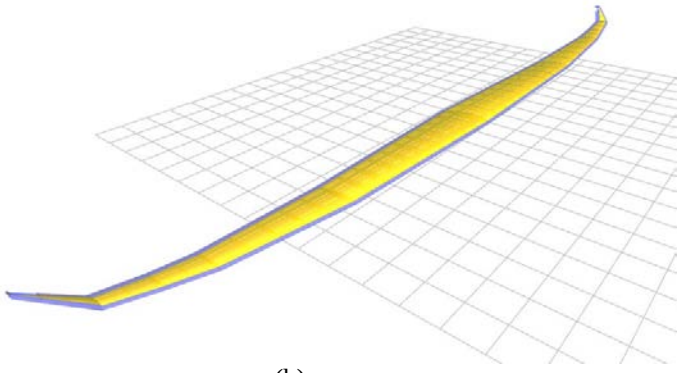

(b)

FIG. 2 3D Wing reconstruction in WingHelper

2.3 Aerodynamic model construction. Constructing the analysis model in XFLR5 [5] represented the most complex stage of the workflow. Based on the previously captured spatial data, the simulation model was synthesized by defining the aircraft's aerodynamic components, including the wing, empennage surfaces and fuselage body, to ensure an accurate representation of the physical airframe.

The wing geometry was built in XFLR5 by entering the chord lengths and positions obtained from the image calibration. Since exact technical drawings were unavailable, the sweep angles and the dihedral seen in Fig. 3 were approximated based on top and front-view photographs. The red line in the 3D view shows the airfoil section, while the wireframe mesh defines the surfaces where the software calculates lift.

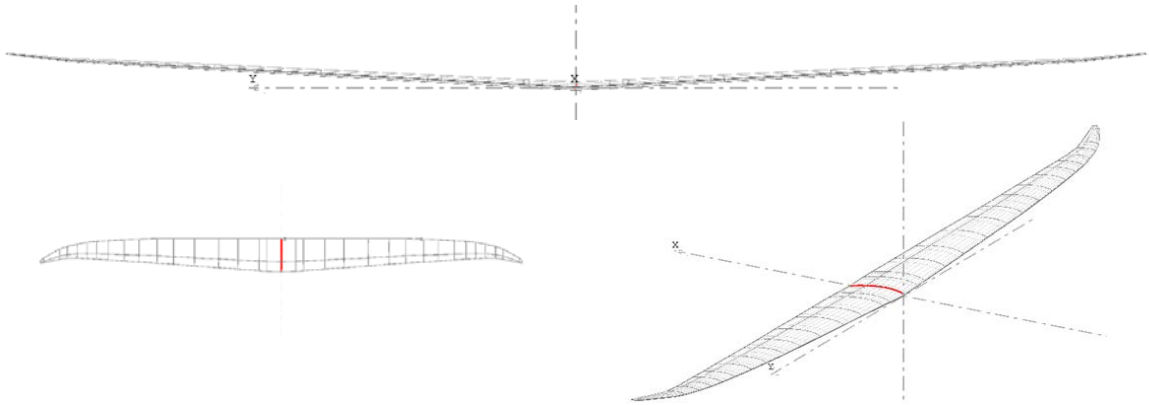

FIG. 3 XFLR5 geometric model of the wing assembly showing front, top and isometric views

A similar process was used for the horizontal stabilizer, as shown in Fig. 4. The span and chord were set according to the digitized measurements, while the overall shape was adjusted to match the visual proportions of the RR Lentus. This model uses a symmetrical profile to ensure the tail remains neutral during flight, which is essential for longitudinal balance.

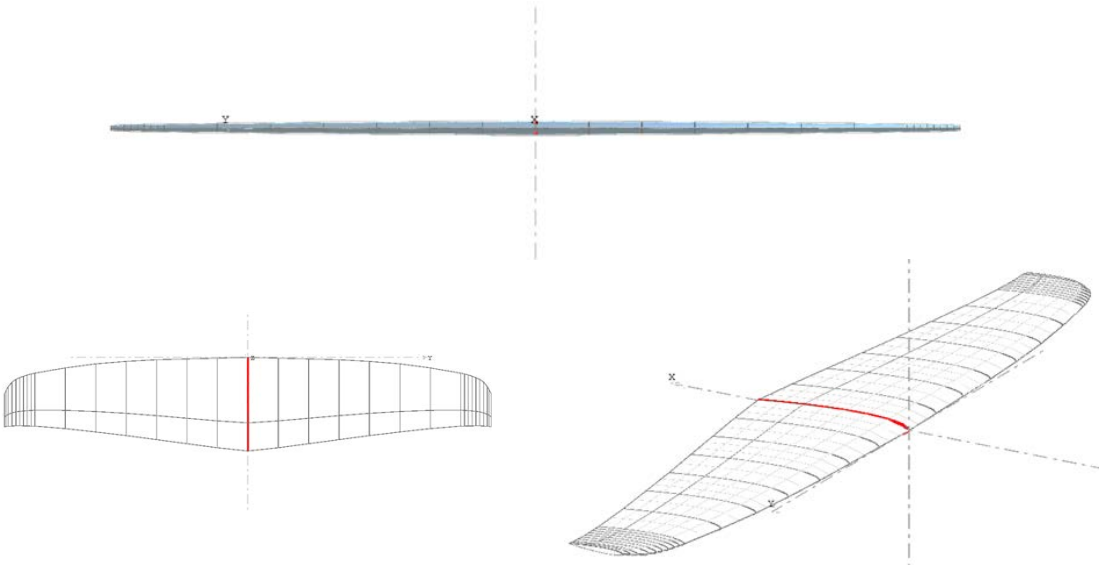

FIG. 4 3D visualization of the elevator assembly in XFLR5, showing the front, top and isometric views

The vertical fin was modeled by defining its height and taper ratio in the XFLR5 geometry editor, as seen in Fig 5. The sweep of the leading edge was approximated to follow the aircraft's scale appearance. This surface provides the necessary directional stability to keep the glider aligned with the airflow during thermal turns.

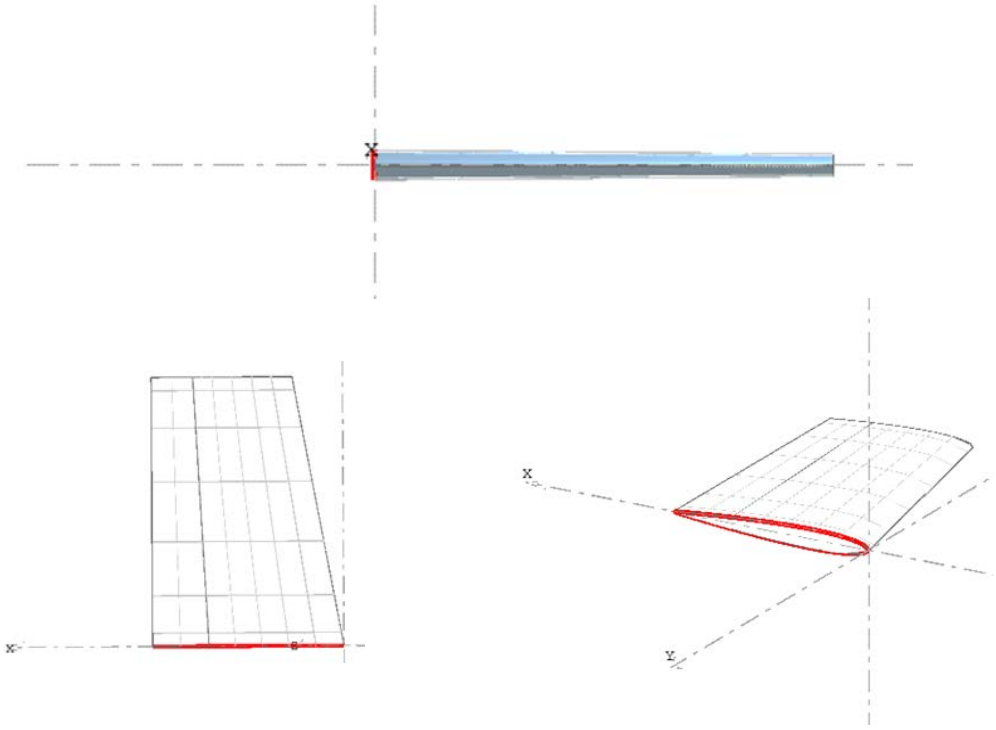

FIG. 5 3D visualization of the fin assembly in XFLR5, showing the front, top and isometric views.

Figure 6 shows the fuselage body, which was created using a series of circular and elliptical cross-sections. These sections were scaled and positioned to replicate the streamlined shape of the real motor glider. Although the fuselage produces very little lift, including it in the model is important for a more realistic estimate of the total drag.

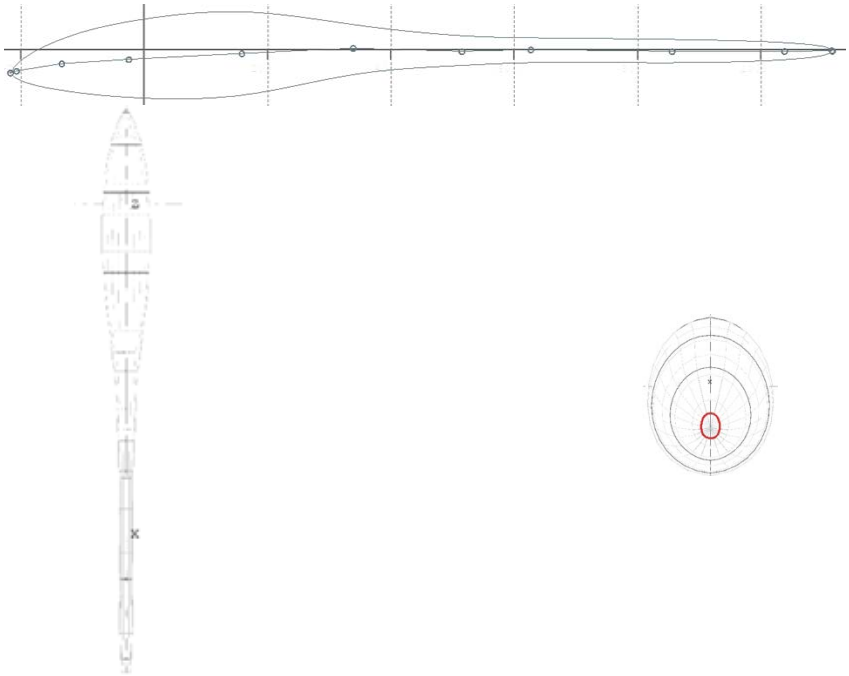

FIG. 6 3D visualization of the body assembly in XFLR5, showing the front, top and isometric views.

The final stage of the geometric reconstruction is the integrated aerodynamic model shown in Fig. 7. This complete digital twin combines the main wing, the empennage and the fuselage into a single computational entity. This unified configuration is used to perform the 3D analysis, allowing for the simulation of complex interactions

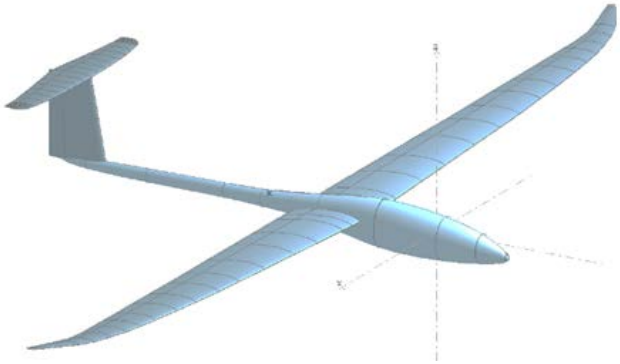

FIG. 7 Complete aerodynamic model definition in XFLR5

3. AERODYNAMIC ANALYSIS

Utilizing the XFLR5 analytical suite, this study evaluated the lift, drag and stability derivatives of the aircraft. The simulation environment was configured to reflect International Standard Atmosphere (ISA) conditions, providing a controlled baseline for the aerodynamic results.

Table 1. Initial conditions for aerodynamic analysis [6, 7].

Parameter	Value	Parameter	Value
Speed	10 m/s	Viscosity	1.46×10^{-5} m^2/s
Air density	1.225 kg/m^3	Method	3D/VLM
AoA interval	-15°÷ 15°, Δ=1°	Reynolds number	108,904 (109,000)
Temperature	15°C	Mach number	0.030 Mach
Aerodynamic airfoils	NACA 4407 (asymmetric) NACA 0009 (symmetric)	MAC	159.37 mm

3.1 Airfoil selection and characteristics. The aerodynamic optimization of the RR Lentus relies on the selection of distinct airfoils for its lifting and stabilizing surfaces. For the main wing, a NACA 4407 (Fig. 8) (modified) was implemented, providing the necessary lift through its 4% camber and 7% thickness to excel in thermal duration flights. This allows for high-alpha maneuvers without the risk of a premature stall. For the empennage, NACA 0009 symmetrical airfoils were adopted [4]. The adoption of a symmetrical section ensures that the stabilizers remain aerodynamically neutral at a 0° angle of attack, preventing unwanted pitching moments and providing a stable reference for the aircraft's longitudinal trim.

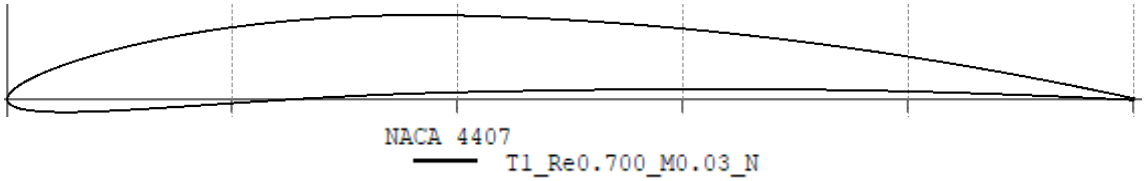

FIG. 8 NACA 4407 airfoil geometry

Analysis of the main wing airfoil NACA 4407

The aerodynamic performance of the main wing is characterized by the polar curves generated in XFLR5.

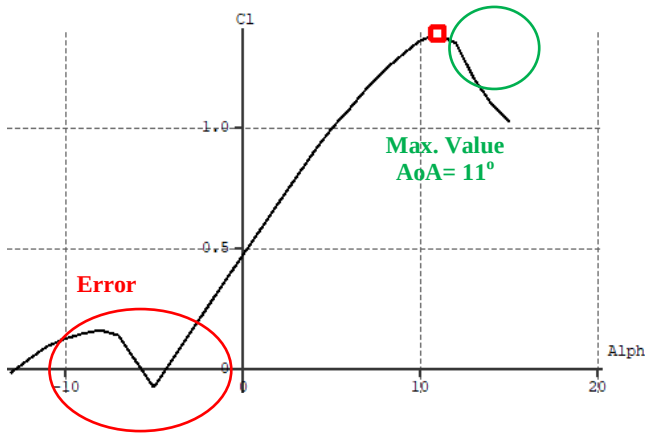

FIG. 9 2D Polar (C_l) for NACA 4407 airfoil computed in XFLR5

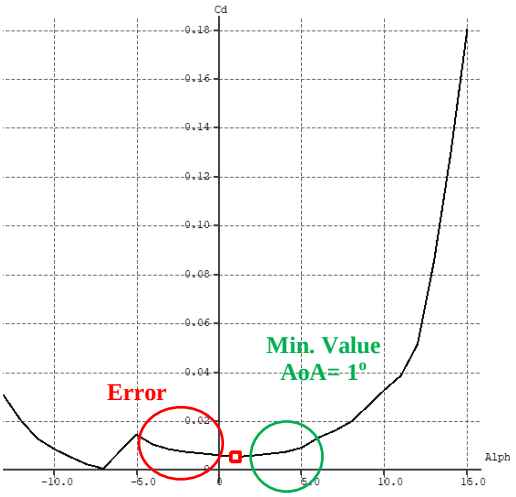

FIG. 10 2D Polar (C_d) for NACA 4407 airfoil computed in XFLR5

Figure 9 illustrates the lift coefficient (C_l) as a function of the angle of attack (α). The curve exhibits a linear behavior typical of cambered airfoils, reaching a maximum lift coefficient (C_{lmax}) of approximately 1.4 at a critical angle of 11°, which represents the stall point.

Figure 10 presents the drag polar, where the low-drag region covers the intended cruising range.

Analysis of the Stabilizer Airfoil (NACA 0009)

The horizontal stabilizer utilizes the symmetrical NACA 0009 (Fig. 11) airfoil to ensure neutral handling characteristics [8, 9].

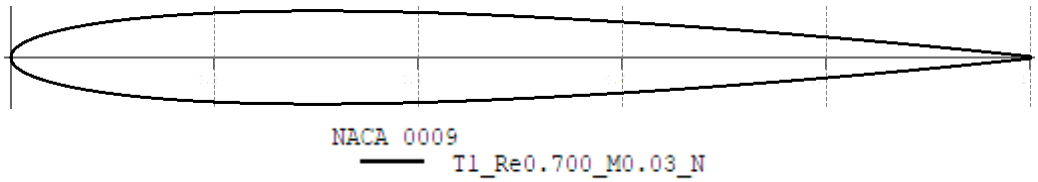

FIG. 11 NACA 0009 airfoil geometry

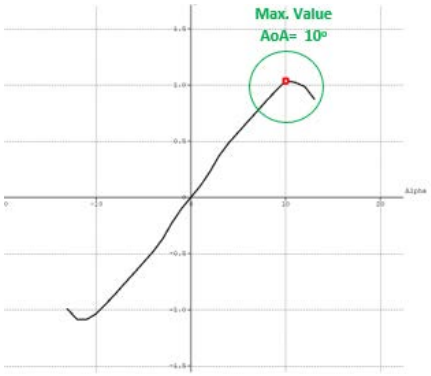

FIG. 12 2D Polar (C_l) for NACA 0009 airfoil computed in XFLR5

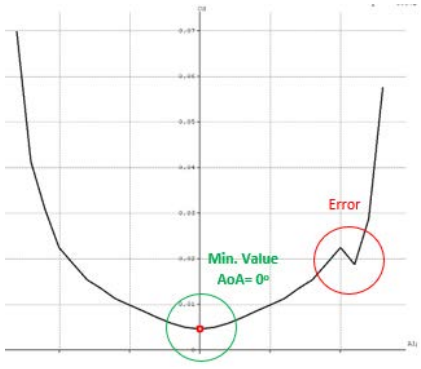

FIG. 13 2D Polar (C_d) for NACA 0009 airfoil computed in XFLR5

As shown in Fig. 12, the lift curve passes directly through the origin (Cl=0 at α=0), confirming that no unintended lift is generated at a neutral angle.

Figure 13 demonstrates that the minimum drag coefficient is also achieved at this 0^o position.

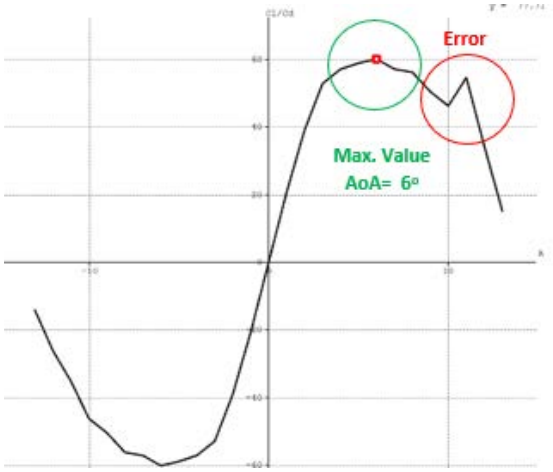

FIG. 14 2D Polar (C_l/C_d) for NACA 0009 airfoil computed in XFLR5

The linear lift slope observed in Fig. 14 ensures predictable pitch authority, allowing for precise control inputs.

3.2 Aerodynamic efficiency (3D wing analysis). The flow visualization in XFLR5 reveals the formation of wingtip vortices and the downwash distribution across the span captured at a fixed angle of attack 5°. However, the irregular behavior of the streamlines at certain chord stations suggests a need for mesh refinement (Fig. 15). To achieve higher numerical convergence and eliminate artificial turbulence, the panel density should be increased and the geometric transitions between the wing segments must be further smoothed to ensure a continuous aerodynamic surface.

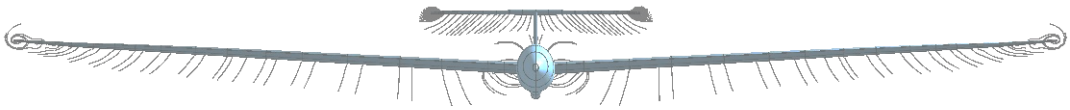

FIG. 15 Visualization of 3D streamlines and wake-vortex distribution for the RR Lentus at a 5° angle of attack in XFLR5

3.3 Longitudinal stability and center of gravity. To establish a reliable baseline for stability, the aircraft's Center of Gravity was derived through a detailed mass-moment analysis of all internal components. By integrating the weights and positions of the motor, battery and servos, the CG was localized at 33% of the chord length relative to the leading edge, it can be seen in Fig. 16. This placement follows the conventional rule for stable RC gliders, providing the necessary restoring moments required for a predictable flight envelope.

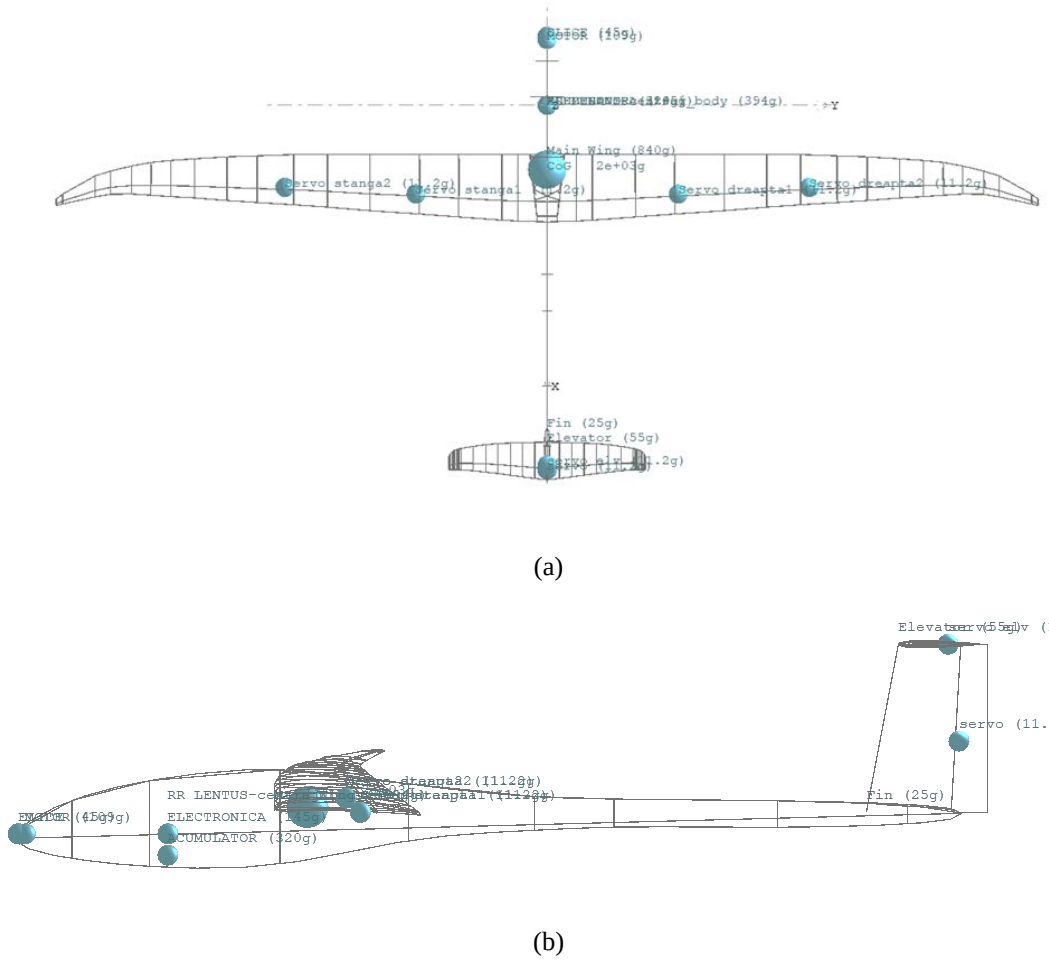

(a)

(b)

FIG. 16 Mass distribution and center of gravity for the RR Lentus: (a) top view and (b) side view

Table 2. List of components and masses

No.	Component	Mass (g)	Type
1	Body (20%)	394	Elapor
2	Main wing (42%)	840	Elapor
3	Fin (2%)	25	Elapor
4	Elevator (3%)	55	Elapor
5	Battery	320	LiPo
6	Electric motor	109	ROXXY brushless
7	Propeller	45	Folding
8	Servo motors (x6)	11.2	HS-65HB
9	Electronics	145	Wiring, ESC, FC, transceiver
TOTAL		2000	

3.4 Full aircraft aerodynamic analysis. The 3D simulation provides a comprehensive evaluation of the complete airframe's performance, accounting for the interaction between lifting surfaces and the resulting aerodynamic forces.

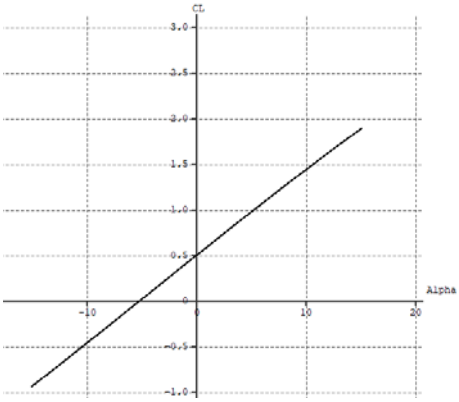

FIG. 17 Variation of lift coefficient (C_L) with angle of attack (α)

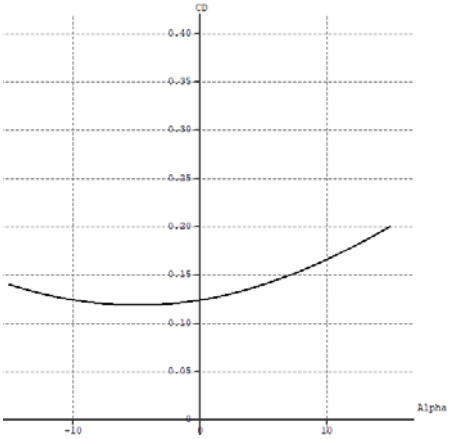

FIG. 18 Variation of drag coefficient (C_D) with angle of attack (α)

Figure 17 illustrates the variation of the total lift coefficient (C_L) as a function of the angle of attack. The curve demonstrates a consistent linear progression within the operational flight envelope, validating the wing's lifting capability. Figure 18 depicts the total drag coefficient (C_D), which represents the effect of parasitic drag (surface friction and form drag) and induced drag. The parabolic nature of this curve highlights the increase in aerodynamic resistance at higher angles of attack, a phenomenon specific to finite wings.

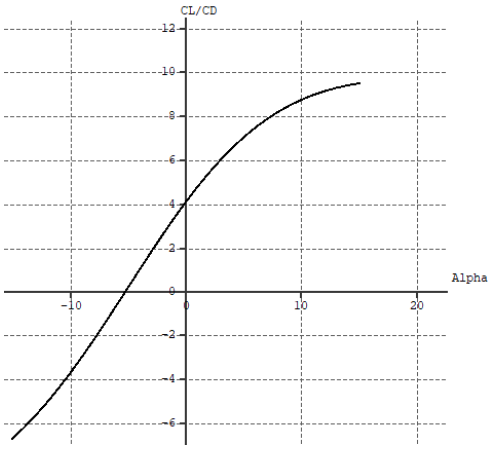

FIG. 19 Variation of lift-to-drag ratio (C_L/C_D) with angle of attack (α)

Figure 19 provides the global lift-to-drag ratio curve, indicating the overall aerodynamic efficiency and the maximum potential gliding range of the RR Lentus.

CONCLUSIONS

This study successfully validated the aerodynamic design and flight characteristics of the RR Lentus motor glider through a comprehensive digital modeling and simulation workflow.

By utilizing ImageOnline for precise geometric extraction, the aircraft was meticulously reconstructed component by component-integrating the main wing, horizontal and vertical stabilizers and the fuselage body-within the XFLR5 environment.

The computational analysis was strategically divided into two phases: initially generating 2D polar curves to evaluate the isolated performance of the NACA 4407 and NACA 0009 airfoils, followed by a full 3D simulation of the complete aerodynamic assembly. The findings confirm that the specific wing configuration yields high aerodynamic efficiency essential for thermal soaring, while the carefully calculated mass balance guarantees inherent longitudinal stability.

Despite these positive outcomes, certain methodological limitations within the simulation framework must be acknowledged. The primary constraint stems from the aerodynamic evaluation relying on XFLR5, an open-source solver based on the Vortex Lattice Method (VLM). While highly effective for preliminary design and standard flight envelopes, this numerical approach is susceptible to convergence artifacts and exhibits reduced accuracy when predicting complex viscous flows, particularly at high angles of attack or in near-stall conditions.

To enhance the precision of future aerodynamic assessments, subsequent research should transition from basic VLM tools to professional-grade Computational Fluid Dynamics (CFD) software capable of accurately modeling flow separation and turbulence. Furthermore, the theoretical 2D airfoil performance and the 3D polar data generated in this study could be physically verified through wind tunnel testing of scaled wing sections. Ultimately, the research would benefit significantly from instrumenting the actual RC aircraft with onboard telemetry sensors. Gathering live data would allow for a direct empirical correlation between the simulated flight parameters and the real-world dynamic behavior, a methodology highly consistent with advanced UAV aerodynamic research [10, 11, 12].

REFERENCES

[1] Multiplex Modellsport, *RR Lentus-Operating Instructions and User Manual*. [Online]. Available: https://www.multiplex-rc.de. [Accessed: January 2026];

[2] ImageOnline.io, *Measure Image Online-Tool for measuring distances and areas in images*. [Online]. Available: https://imageonline.io/measure-image. [Accessed: February 2026];

[3] WingHelper, *WingHelper 1.5 - Parametric 3D Wing Design Software, Official Documentation*. [Online]. Available: https://www.winghelper.com. [Accessed: December 2024];

[4] Airfoil Tools, *Airfoil Database and NACA Airfoil Generator*. [Online]. Available: http://airfoiltools.com. [Accessed: December 2024];

[5] A. Deperrois, *XFLR5 v6.61-Analysis of foils and wings operating at low Reynolds numbers, Guidelines for VLM implementation*. [Online]. Available: http://www.xflr5.tech. [Accessed: December 2024];

[6] AeroToolbox, *Standard Atmosphere Calculator-Online Tool for Calculation of Standard Atmosphere Properties*. [Online]. Available: https://aerotoolbox.com/atmcalc/. [Accessed: February 2026];

[7] Airfoil Tools, *Reynolds Number Calculator-Online Tool for Reynolds Number Estimation*. [Online]. Available: http://airfoiltools.com/calculator/reynoldsnumber. [Accessed: February 2026];

[8] V. B. Mohan, Design and Hydrodynamic Analysis of an Autonomous Hydrofoil Catamaran: Enhancing Efficiency and Performance through Predictive Control, *Technical Report*, 2024. [Online]. Available: https://www.researchgate.net/publication/382453171_Design_and_Hydrodynamic_Analysis_of_an_Autonomous_Hydrofoil_Catamaran_Enhancing_Efficiency_and_Performance_through_Predictive_Control. [Accessed: January 2026];

[9] Y. F. Görgülü, M. A. Özgür and R. Köse, CFD analysis of a NACA 0009 aerofoil at a low reynolds number, *Journal of Polytechnic*, vol. 24, no. 3, 2021. [Online]. Available: https://dergipark.org.tr/en/download/article-file/1566645. [Accessed: January 2026];

[10] V. Prisacariu, Analysis of UAVs flight characteristics, *Review of the Air Force Academy*, vol. 38, no. 3, pp. 29-36, 2018. DOI: 10.19062/1842-9238.2018.16.3.4;

[11] V. Prisacariu and L. Simionescu, Flight performance analysis for UAVs-MFD NIMBUS, in *Scientific Research and Education in the Air Force - AFASES 2018*, Brașov, Romania, 2018, pp. 225-232. DOI: 10.19062/2247-3173;

[12] V. Prisacariu and A. Chirilă, Aerodynamic Analysis of Helicopter Fenestron Vertical Tail, in *Scientific Research and Education in the Air Force-AFASES 2019*, Brașov, Romania, 2019. [Online]. Available: https://doi.org/10.19062/2247-3173.2019.21.24.

ANNEXES

Annex 1. Calculated Polars for NACA 0009 Airfoil

Calculated polar for: NACA 0009

1 1 Reynolds number fixed Mach number fixed

xtrf = 1.000 (top) 1.000 (bottom)
Mach = 0.030 Re = 0.700 e 6 Ncrit = 9.000

alpha	CL	CD	CDp	Cm	Top Xtr	Bot Xtr	Cpmin	Chinge	XCp		
-13.000	-0.9920	0.06973	0.06745	-0.0066	1.0000	0.0110	-7.9357	-0.0076	0.0007	-0.0664	0.2301
-12.000	-1.0822	0.04130	0.03811	-0.0246	1.0000	0.0109	-8.6791	-0.0048	-0.0011	-0.0454	0.2158
-11.000	-1.0858	0.03087	0.02666	-0.0167	1.0000	0.0114	-8.3231	-0.0048	-0.0034	-0.0490	0.2244
-10.000	-1.0355	0.02244	0.01729	-0.0110	1.0000	0.0126	-7.5551	-0.0049	-0.0043	-0.0507	0.2303
-9.000	-0.9504	0.01888	0.01335	-0.0079	1.0000	0.0145	-6.4679	-0.0048	-0.0047	-0.0487	0.2338
-8.000	-0.8622	0.01537	0.00948	-0.0046	1.0000	0.0176	-5.4510	-0.0047	-0.0049	-0.0467	0.2378
-7.000	-0.7660	0.01343	0.00734	-0.0021	1.0000	0.0212	-4.3867	-0.0045	-0.0050	-0.0437	0.2414
-6.000	-0.6738	0.01123	0.00497	0.0014	1.0000	0.0299	-3.4998	-0.0045	-0.0051	-0.0422	0.2470
-5.000	-0.5787	0.00984	0.00359	0.0046	1.0000	0.0491	-2.6763	-0.0045	-0.0050	-0.0402	0.2536
-4.000	-0.4844	0.00850	0.00262	0.0077	1.0000	0.1290	-1.9720	-0.0045	-0.0049	-0.0383	0.2623
-3.000	-0.3726	0.00706	0.00200	0.0065	0.9965	0.3260	-1.3384	-0.0035	-0.0047	-0.0303	0.2645
-2.000	-0.2269	0.00582	0.00160	-0.0015	0.9828	0.5554	-0.7951	-0.0008	-0.0046	-0.0112	0.2407
-1.000	-0.1020	0.00493	0.00137	-0.0038	0.9466	0.7369	-0.4758	0.0006	-0.0056	-0.0001	0.2104
0.000	0.0000	0.00458	0.00128	-0.0000	0.8666	0.8666	-0.3120	-0.0000	-0.0054	0.0002	0.4852
1.000	0.1020	0.00493	0.00137	0.0038	0.7369	0.9466	-0.4758	-0.0006	-0.0056	0.0006	0.2104
2.000	0.2269	0.00582	0.00160	0.0015	0.5553	0.9828	-0.7951	0.0008	-0.0046	0.0116	0.2407
3.000	0.3726	0.00706	0.00200	-0.0065	0.3260	0.9965	-1.3384	0.0035	-0.0047	0.0307	0.2645
4.000	0.4844	0.00850	0.00261	-0.0077	0.1290	1.0000	-1.9718	0.0045	-0.0049	0.0387	0.2622
5.000	0.5786	0.00984	0.00358	-0.0046	0.0491	1.0000	-2.6761	0.0045	-0.0050	0.0406	0.2536
6.000	0.6737	0.01123	0.00497	-0.0013	0.0299	1.0000	-3.4997	0.0045	-0.0050	0.0425	0.2470
7.000	0.7660	0.01343	0.00734	0.0021	0.0212	1.0000	-4.3867	0.0045	-0.0050	0.0441	0.2414
8.000	0.8623	0.01537	0.00948	0.0046	0.0175	1.0000	-5.4512	0.0047	-0.0048	0.0471	0.2378
9.000	0.9505	0.01888	0.01335	0.0079	0.0145	1.0000	-6.4683	0.0048	-0.0046	0.0490	0.2338
10.000	1.0356	0.02244	0.01729	0.0109	0.0126	1.0000	-7.5558	0.0049	-0.0043	0.0510	0.2304
11.000	1.0209	0.01872	0.01480	0.0221	0.0116	1.0000	-7.8827	0.0040	-0.0030	0.0411	0.2186
12.000	0.9839	0.02870	0.02561	0.0308	0.0112	1.0000	-8.0445	0.0043	-0.0001	0.0384	0.2077
13.000	0.8744	0.05745	0.05509	0.0185	0.0115	1.0000	-7.2981	0.0059	0.0005	0.0517	0.2164

Annex 2. NACA 4407 2D Airfoil Analysis

Calculated polar for: NACA 4407

1 1 Reynolds number fixed Mach number fixed

xtrf = 1.000 (top) 1.000 (bottom)
Mach = 0.030 Re = 0.700 e 6 Ncrit = 9.000

alpha	CL	CD	CDp	Cm	Top Xtr	Bot Xtr	Cpmin	Chinge	XCp		
-13.000	-0.0139	0.03020	0.02867	-0.0595	0.9820	0.0121	-0.5032	0.0054	0.0020	0.0402	-3.8825
-12.000	0.0424	0.02041	0.01886	-0.0703	0.9719	0.0121	-0.5204	0.0071	0.0030	0.0524	1.8587
-11.000	0.0939	0.01286	0.01132	-0.0770	0.9507	0.0142	-0.4113	0.0080	0.0034	0.0607	1.0478
-10.000	0.1250	0.00857	0.00699	-0.0806	0.9254	0.0175	-0.4318	0.0080	0.0033	0.0637	0.8795
-9.000	0.1470	0.00523	0.00362	-0.0845	0.8971	0.0188	-0.5985	0.0079	0.0031	0.0657	0.8128
-8.000	0.1609	0.00221	0.00057	-0.0883	0.8625	0.0175	-0.9457	0.0078	0.0027	0.0671	0.7885
-7.000	0.1399	0.00041	-0.00127	-0.0957	0.8307	0.0159	-1.5872	0.0077	0.0023	0.0676	0.9244
-5.000	-0.0757	0.01432	0.00999	-0.1087	0.9637	0.0102	-4.2423	0.0086	0.0037	0.0667	-1.2038
-4.000	0.0345	0.01028	0.00515	-0.1085	0.9397	0.0149	-3.2582	0.0090	0.0041	0.0734	3.4296
-3.000	0.1436	0.00828	0.00278	-0.1076	0.9097	0.0241	-2.2139	0.0093	0.0044	0.0795	1.0042
-2.000	0.2534	0.00724	0.00162	-0.1068	0.8726	0.0571	-1.4559	0.0096	0.0046	0.0856	0.6731
-1.000	0.3628	0.00660	0.00118	-0.1062	0.8264	0.1932	-0.7280	0.0100	0.0048	0.0916	0.5431
1.000	0.5761	0.00516	0.00117	-0.1041	0.7039	1.0000	-0.6760	0.0110	0.0047	0.1005	0.4293
2.000	0.6843	0.00569	0.00136	-0.1033	0.6336	1.0000	-0.7648	0.0117	0.0064	0.1057	0.3989
4.000	0.8962	0.00720	0.00233	-0.1015	0.4703	1.0000	-1.6831	0.0129	0.0071	0.1192	0.3593
5.000	0.9936	0.00895	0.00331	-0.0994	0.2857	1.0000	-2.6603	0.0132	0.0074	0.1232	0.3452
6.000	1.0736	0.01306	0.00603	-0.0950	0.0210	1.0000	-3.6271	0.0129	0.0073	0.1224	0.3326
7.000	1.1612	0.01592	0.00918	-0.0910	0.0108	1.0000	-4.4765	0.0129	0.0075	0.1234	0.3213
8.000	1.2372	0.01970	0.01334	-0.0852	0.0085	1.0000	-5.6174	0.0127	0.0076	0.1220	0.3106
9.000	1.2997	0.02604	0.02016	-0.0780	0.0073	1.0000	-6.8256	0.0124	0.0078	0.1190	0.3005
10.000	1.3580	0.03260	0.02749	-0.0708	0.0060	1.0000	-8.0358	0.0122	0.0081	0.1163	0.2913
11.000	1.3830	0.03851	0.03404	-0.0600	0.0043	1.0000	-9.0019	0.0117	0.0087	0.1087	0.2811
12.000	1.3460	0.05133	0.04780	-0.0483	0.0039	1.0000	-9.0782	0.0124	0.0113	0.1050	0.2722
13.000	1.2028	0.08551	0.08326	-0.0516	0.0044	1.0000	-7.1749	0.0147	0.0143	0.1236	0.2778
14.000	1.0956	0.12923	0.12755	-0.0775	0.0049	1.0000	-5.8745	0.0164	0.0160	0.1382	0.3049
15.000	1.0243	0.18009	0.17835	-0.1011	0.0061	1.0000	-3.6111	0.0175	0.0173	0.1476	0.3330

Annex 3. Mass and inertia distribution

```
x,y,z system here must be exactly the same one used in the .avl input file
   (same orientation, same origin location, same length units)

   mass          x          y          z        Ixx        Iyy        Izz        Ixy        Ixz        Iyz
    840        225  -1.67e-13       31.3      0.333     0.0017      0.334          0  -0.000137          0 ! Main Wing
     55   1.07e+03   -5.5e-14        236    0.00111   2.84e-05    0.00114          0   9.32e-11          0 ! Elevator
     25   1.06e+03  -6.52e-05        106   0.000113   0.000146   3.25e-05          0   1.25e-05          0 ! Fin
    394        285          0      -7.45   2.34e-05     0.0415     0.0414          0   0.000737          0 ! Body's inertia
   11.2        250        800         20      0.000      0.000      0.000 ! Servo dreapta2
   11.2        270        400          0      0.000      0.000      0.000 ! Servo dreapta1
   11.2        270       -400          0      0.000      0.000      0.000 ! Servo stanga1
   11.2        250       -800         20      0.000      0.000      0.000 ! Servo stanga2
   11.2   1.1e+03          0        236      0.000      0.000      0.000 ! servo elv
   11.2  1.11e+03          0        100      0.000      0.000      0.000 ! servo
    109       -200          0        -30      0.000      0.000      0.000 ! MOTOR
    320          0          0        -60      0.000      0.000      0.000 ! ACUMULATOR
     45       -210          0        -30      0.000      0.000      0.000 ! ELICE
    145          0          0        -30      0.000      0.000      0.000 ! ELECTRONICA
```

Annex 4. 3D Analysis of the Balanced Model

```
Plane name :        RR LENTUS-centraj 4415
Polar name :        T1-10.0 m/s-VLM2
Freestream speed :  10.000 m/s
```

alpha	Beta	CL	CDi	CDv	CD	CY	Cl	Cm	Cn	Cni	QInf	XCP
-15.000	0.000	-0.933247	0.022451	0.117105	0.139556	-0.000040	-0.000005	0.019282	0.000006	0.000007	10.0000	0.3094
-14.000	0.000	-0.839335	0.018537	0.117105	0.135642	-0.000040	-0.000004	0.042079	0.000006	0.000007	10.0000	0.3127
-13.000	0.000	-0.744925	0.014986	0.117105	0.132091	-0.000040	-0.000004	0.064196	0.000006	0.000007	10.0000	0.3170
-12.000	0.000	-0.650067	0.011814	0.117105	0.128918	-0.000040	-0.000004	0.085605	0.000006	0.000007	10.0000	0.3226
-11.000	0.000	-0.554810	0.009030	0.117105	0.126135	-0.000040	-0.000004	0.106279	0.000006	0.000006	10.0000	0.3303
-10.000	0.000	-0.459204	0.006648	0.117105	0.123753	-0.000040	-0.000004	0.126193	0.000006	0.000006	10.0000	0.3413
-9.000	0.000	-0.363298	0.004675	0.117105	0.121780	-0.000040	-0.000004	0.145322	0.000006	0.000006	10.0000	0.3583
-8.000	0.000	-0.267144	0.003121	0.117105	0.120226	-0.000039	-0.000003	0.163642	0.000006	0.000006	10.0000	0.3877
-7.000	0.000	-0.170794	0.001992	0.117105	0.119097	-0.000039	-0.000003	0.181131	0.000006	0.000006	10.0000	0.4504
-6.000	0.000	-0.074300	0.001294	0.117105	0.118399	-0.000039	-0.000003	0.197766	0.000006	0.000006	10.0000	0.6763
-5.000	0.000	0.022288	0.001033	0.117105	0.118138	-0.000039	-0.000003	0.213528	0.000006	0.000006	10.0000	-1.0575
-4.000	0.000	0.118915	0.001210	0.117105	0.118315	-0.000038	-0.000003	0.228396	0.000006	0.000006	10.0000	0.0262
-3.000	0.000	0.215530	0.001828	0.117105	0.118933	-0.000038	-0.000003	0.242351	0.000006	0.000006	10.0000	0.1383
-2.000	0.000	0.312081	0.002887	0.117105	0.119992	-0.000038	-0.000003	0.255377	0.000006	0.000006	10.0000	0.1810
-1.000	0.000	0.408514	0.004386	0.117105	0.121491	-0.000037	-0.000002	0.267457	0.000006	0.000006	10.0000	0.2035
0.000	0.000	0.504777	0.006323	0.117105	0.123428	-0.000037	-0.000002	0.278575	0.000005	0.000006	10.0000	0.2175
1.000	0.000	0.600819	0.008695	0.117105	0.125800	-0.000037	-0.000002	0.288717	0.000005	0.000006	10.0000	0.2270
2.000	0.000	0.696586	0.011496	0.117105	0.128601	-0.000036	-0.000002	0.297872	0.000005	0.000005	10.0000	0.2339
3.000	0.000	0.792027	0.014721	0.117105	0.131826	-0.000036	-0.000002	0.306026	0.000005	0.000005	10.0000	0.2392
4.000	0.000	0.887092	0.018362	0.117105	0.135467	-0.000035	-0.000002	0.313169	0.000005	0.000005	10.0000	0.2434
5.000	0.000	0.981729	0.022409	0.117105	0.139514	-0.000035	-0.000002	0.319293	0.000005	0.000005	10.0000	0.2468
6.000	0.000	1.075888	0.026854	0.117105	0.143959	-0.000034	-0.000002	0.324388	0.000005	0.000005	10.0000	0.2497
7.000	0.000	1.169519	0.031684	0.117105	0.148789	-0.000034	-0.000001	0.328449	0.000005	0.000005	10.0000	0.2521
8.000	0.000	1.262574	0.036888	0.117105	0.153993	-0.000033	-0.000001	0.331469	0.000004	0.000005	10.0000	0.2542
9.000	0.000	1.355005	0.042452	0.117105	0.159557	-0.000033	-0.000001	0.333445	0.000004	0.000005	10.0000	0.2561
10.000	0.000	1.446764	0.048360	0.117105	0.165465	-0.000032	-0.000001	0.334374	0.000004	0.000004	10.0000	0.2578
11.000	0.000	1.537805	0.054597	0.117105	0.171702	-0.000031	-0.000001	0.334253	0.000004	0.000004	10.0000	0.2593
12.000	0.000	1.628082	0.061147	0.117105	0.178252	-0.000031	-0.000001	0.333082	0.000004	0.000004	10.0000	0.2608
13.000	0.000	1.717552	0.067991	0.117105	0.185096	-0.000030	-0.000001	0.330862	0.000004	0.000004	10.0000	0.2621
14.000	0.000	1.806171	0.075110	0.117105	0.192215	-0.000030	-0.000001	0.327596	0.000004	0.000004	10.0000	0.2633
15.000	0.000	1.893897	0.082485	0.117105	0.199590	-0.000029	-0.000001	0.323286	0.000004	0.000004	10.0000	0.2644